Fourth Tetons Conference: Galactic Structure, Stars, and the Interstellar Medium
ASP Conference Series, Vol. 000, 2000
M.D. Bicay & C.E. Woodward

The McKee/Ostriker Model: Paradigm?

Presented at The Fourth Tetons Summer Conference: Galactic Structure, Stars, and the Interstellar Medium

Carl Heiles
Astronomy Department, University of California, Berkeley, CA 94720-3411

Abstract. We summarize the current observational status of the interstellar medium in terms of the McKee/Ostriker model. We find both agreement and disagreement—hence the title of the paper. Some of the newest observations differ from older ones, which underscores the need for both more and better data.

1. Introduction

In 1977 Mckee & Ostriker (MO) extended the two-phase model of Field, Goldsmith, & Habing (1969; FGH) by including supernova and wrote their famous paper entitled "A theory of the interstellar medium - Three components regulated by supernova explosions in an inhomogeneous substrate". Their ISM is dominated by individual supernova (SN) explosions; today some believe we should replace the individual explosions by correlated ones producing superbubbles. The Hot Ionized Medium (HIM) fills the interior of SN remnants and powers their blast waves, which sweep up the gas and magnetic field inside the bubble and pile them into the shell. Soon this shocked gas starts to cool and recombine rapidly, forming the Cold Neutral Medium (CNM) with an amplified field. Soft X-rays produced by immediately adjacent HIM penetrate the outsides of CNM clouds, heating the gas to form the partially ionized Warm Neutral Medium (WNM), whose more partially ionized portions are the Warm Ionized Medium (WIM). Their model is impressive in its physical development and internal consistency. It makes many predictions and stands as the accepted paradigm against which most discussions and interpretations are compared.

The FGH and MO models rely on a broad range of physical processes, ranging from atomic interactions with energetic particles to gasdynamics, and the uninitiated may be easily overwhelmed. Fortunately, there is a straightforward path to nirvana, namely excellent, classical reviews that remain useful for experts. Dalgarno & McCray (1972) present the physics of heating and cooling for atomic regions, the basis for the FGH model. MO's paper is a bit intimidating for many of us, but their Figures 1 → 3 and Table 1 present an excellent three-minute overview of the basic picture. McCray & Snow (1979) present a highly readable discussion of the details and basic physics behind all aspects of the MO

model, together with some critical comments that remain relevant today. At the first Tetons meeting, Kulkarni & Heiles (1987; KH) interpreted ISM observations of the cool and warm phases in terms of the MO paradigm with great success. Cox (1995) presents a historical overview of our ISM understanding, and lack of it, and emphasizes some specific problems with the MO model.

The MO model doesn't cover everything. The magnetic field and cosmic rays play important roles in the overall dynamics of the ISM. Their pressures are larger than the typically adopted thermal pressures of the gas components. Even for the large-scale z-distribution, where the pressure gradients may be small, their pressures contribute to the hydrostatic balance (Boulares & Cox 1990). Also, the magnetic field links the different gas phases with each other, and also with the cosmic rays, so that components cannot act independently. Rather, analysis of the dynamics and equilibria must include the whole ensemble, and this leads to new modes of behavior such as magnetically-linked clouds (Elmegreen 1994) and the Parker (1966) instability. As important as these two nonthermal, non-material components are, we will not emphasize them in this review.

Rather, we will define and review *five* (not MO's three) diffuse gas phases. These are the HIM, the HII-region like Reynolds WIM (RWIM), the MO-like WIM (MOWIM), the WNM, and the CNM. We begin with a definition of and brief introduction to the five phases in §2 and then go on to discuss various aspects in more detail.

2. Introduction to the Five ISM Phases

Table 1 presents the essential properties of the five diffuse gas phases. The tabular form inspires confidence, but this is misleading because there is uncertainty and disagreement; the table reflects my personal bias. Perhaps most blatant, the idea that the MOWIM is an observationally important phase that contributes most of the total electron column is not (yet?) widely accepted.

Table 1. THE DIFFUSE ISM PHASES

Quantity	HIM	RWIM	WNM/MOWIM	CNM
h T, K	$?\rightarrow 10^7$	~ 8000	$500 \rightarrow 8000^A$	$10 \rightarrow 75^A$
$\frac{P}{k}$, cm^{-3} K	$\gtrsim 20000^B$	$\gtrsim 3400^B$	$200? \rightarrow 4000^A$	$1500 \rightarrow 10000$
n, cm^{-3}	0.003	~ 0.08	$0.1 \rightarrow 0.4^A$	$20 \rightarrow 250$
X_e	1	1	$\sim 10^{-2} \rightarrow 0.5^A$	$\sim 2\times 10^{-4}$ $(=\frac{C}{H})$
f	0.5^C	0.1^C	0.5^C	0.01^C
$N_{20\perp}$	$\sim 0.3?^E$	$0.1?^E$	H, 1.9; e, $0.3?^E$	1.8
Heating	shocks	H photoion + ?	grains, etc^D	C ionization, etc^D
Ionization	el coll	H photoion	H XR, some CR	C photoion, some CR
Observing	XR, UVa, UVe	DM, EM, SM, UVa, FS	HIem, UVa,IRe, FS	HIe, HIa, UVa, IRe, FS

In column 1, X_e is the ionization fraction $\frac{n_e}{n_e+n_{HI}}$; f is volume filling fraction; $N_{20\perp}$ is the H or electron column density projected towards the Galactic pole in units of 10^{20} cm^{-3}. In other columns, XR is X-Ray emission; DM pulsar dispersion; EM Hα emission; SM pulsar scattering; FS fine structure lines in emission; IRe continuum IR emission from grains; UVa optical/UV absorption lines against stars; UVe UV emission lines; HIe and HIa 21-cm line emission and absorption.

[A] This quantity is critically discussed herein and these values may be either not correct or not generally accepted.

[B] These are typical pressures; wide fluctuations exist.

[C] Volume filling factors depend on z and are highly uncertain; these values are for $z = 0$.

[D] In contrast to the other phases, multiple heating mechanisms are important for the WNM and CNM; see Figure 3 of Wolfire et al (1995a).

[E] The N_e $\perp$ for the HIM is a theoretical value (Wolfire et al 1995b). The relative contributions of the RWIM and the MOWIM to $N_{e,\perp}$ are abritrarily chosen and are highly uncertain (§5).

2.1. Introduction to the HIM

The HIM is produced by SN shocks and resides in SN remnants and superbubbles. It can be mapped with its X-ray emission. Cooler remnants can be observed with 0.25 keV X rays if the intervening HI column density is low enough ($N_{HI,20} \lesssim 0.6$, where $N_{HI,20}$ is the HI column density in units of 10^{20} cm^{-2}). This is tiny, so even the thinnest cloud obscures the 0.25 keV emission. Higher energies are easier because the HI opacity is much smaller; for example, for $T \gtrsim 2 \times 10^6$ K the 0.75 keV emission can be seen through $N_{HI,20} \lesssim 20$. Even this is serious for locating distant objects because this column of HI is normally accumulated over a path length ~ 700 pc, so we can only map nearby structures, of which there are two prominent ones: the North Polar Spur and the Eridanus superbubble. The ROSAT satellite's all-sky X-ray maps for 0.25, 0.75, and 1.5 keV (Snowden et al 1997) are the best available.

Gas having $T \lesssim 0.7 \times 10^6$ K must exist, because the HIM cools down as it ages. But such cool gas cannot be seen with X rays. UV absorption lines of the He$^+$-like ions OVI, NVI, and CIV trace HIM at temperatures $\sim 3 \times 10^5$ K and below. Such lines provide velocity resolution and column density, which greatly helps the interpretation (e.g. Shelton & Cox 1994).

These lines can also be seen—weakly—in emission, which provides the emission measure instead of column density, so a comparison of absorption and emission provides the electron density n_e. OVI emission reveals gas at $T \sim 3 \times 10^5$ K and implies high pressures, $\frac{P}{k} \sim 40000$ cm^{-3} K (Dixon, Davidsen, & Ferguson 1996) while CIV reveals $T \sim 10^5$ K and implies much lower pressures, $\frac{P}{k} \sim 2000$ cm^{-3} K (Martin & Bowyer 1990). Both datasets are noisy and sample only a few sightlines, so these results should be regarded as provisional.

2.2. Introduction to the Reynolds WIM (RWIM)

The RWIM is widely distributed, HII-like highly ionized gas having $n_e \sim 0.08$ cm^{-3} and $T \sim 8000$ K (Haffner, Reynolds, & Tufte 1999). The RWIM is often called the "Reynolds layer", after the person who has pursued its study most vigorously; the culmination is the WHAM survey, which provides the Galactic Hα data cube for most of the sky (Haffner, this meeting). Its ionization requires a significant continuing energy input; for conventional sources only starlight is sufficient (Reynolds 1984), and despite concerns about how the starlight penetrates neutral regions, it seems theoretically possible and the RWIM can be described as HII region envelopes (Miller & Cox 1993; Dove & Shull 1994; McKee & Williams 1997; Anantharamaiah 1985, 1986). In §3.1 we extrapolate from the Eridanus superbubble and argue that much of the RWIM is formed by ionization of supershell walls by stellar UV photons from the OB clusters inside.

The question mark under RWIM heating in Table 1 refers to a possible extra heating component required to explain observed RWIM temperatures at high $|z|$ (Reynolds, Haffner, & Tufte 1999).

Taylor & Cordes (1993; TC) use pulsar DM's to derive the standard model of electron distribution in the Galaxy. They use the implicit assumption that pulsar DM's are produced by the RWIM; in contrast, we argue below that the DM's are produced mainly by the MOWIM (see below). The RWIM can also be observed with IR fine structure emission lines (e.g. Heiles 1994).

2.3. Introduction to the MOWIM

MO predicted this phase, considering it simply as partially ionized WNM. However, if it really produces most of the observationally important pulsar DM's, then we believe its status should be elevated and considered as a separate phase. In §4 and 5 we discuss Hα, pulsar, and optical/UV absorption line data in some detail and argue that, indeed, a significant fraction of the pulsar DM-producing electrons does reside in the MOWNM. The idea that the WNM contributes significantly to pulsar dispersion is contrary to current observational thought—but in agreement with MO.

2.4. Introduction to the WNM and CNM

In the MO model, the CNM resides in the walls of SN remnant walls. Soft X-rays produced by the adjacent HIM penetrate the outside layer of CNM clouds, heating and partially ionizing the gas to form the WNM; in our parlance, this partially-ionized WNM is the MOWIM. Thus the swept-up gas consists of two distinct neutral phases, each in thermally stable equilibrium and with thermal pressures at least roughly equal. The shells can break up, forming clouds, and these in turn can be overcome by a different passing SN shock, placing them inside either a SN remnant or a superbubble wall.

The CNM and WNM temperatures are derived by calculating the equilibrium temperature as a function of thermal pressure. With this formulation and realistic heating and cooling functions there exist two stable ranges of equilibrium, the CNM and the WNM with temperatures ~ 50 and ~ 8000 K, separated by a region of unstable temperatures. *Stable* thermal pressure equilibrium, and thermal pressure equality between physically adjacent phases, is a cornerstone of the MO theory, although the pressure varies widely from one region to another, as observed (Jenkins, Jura, & Lowenstein 1983). In §6.3, we find that a significant population of WNM lies at thermally *unstable* temperatures—contrary to MO.

The 21-cm line in emission maps the total HI column density, both the WNM and the CNM, in the usual case when the opacity is not too high. The latest survey of the northern sky is Hartmann & Burton (1997), with 36 arcmin resolution. The opacity $\propto \frac{1}{T}$, and the large temperature difference between WNM and CNM means that, in effect, only the CNM is seen in absorption spectra against background continuum sources. We defer discussing 21-cm line and optical/UV absorption line data to §6.

IR emission from grains is a reasonably accurate tracer of total column density of gas, including not only the atomic components but also the ionized

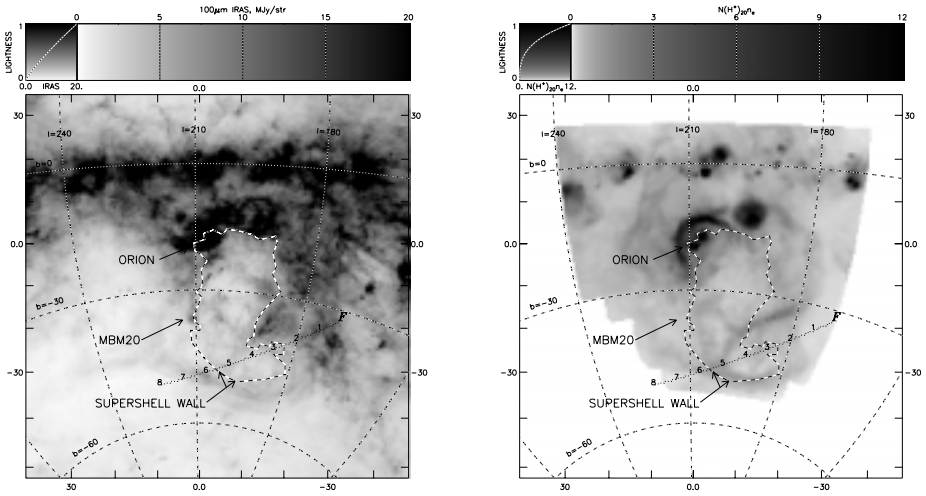

Figure 1. The Eridanus regions mapped in *(left)* 100 μm emission from IRAS, which traces mainly atomic and molecular hydrogen, and *(right)* Hα emission from the WHAM survey. The heavy dashed line labeled "SUPERSHELL WALL" outlines the boundary of the 0.75 keV emission, which is very sharp. The grey scales are calibrated by the colorbars on top right of each panel; saturated parts of the images exceed the colorbar maxima. Galactic coordinates are labeled on the dashed grid lines. Larger versions are in Heiles et al (1999).

and molecular components; the most useful is the 100 μm IRAS maps (e.g. Schlegel, Finkbeiner, & Davis 1998).

The physically most interesting tracer is the 158 μm fine structure line of C^+, because this is the principal coolant. Maps of this line, with sufficient sensitivity and velocity resolution to distinguish WNM from CNM, would be of great value in developing our understanding of the physical processes in these phases. The only current data on local gas are Matsuhara et al (1997), and even though they have insufficient velocity resolution, they are valuable in providing accurate cooling rates. Nakagawa et al (1998) provide a large-scale survey of the interior Galactic plane.

3. The ISM and Superbubbles

3.1. The Eridanus Superbubble

The Eridanus superbubble has been studied previously by several groups; the description below is a brief version of Heiles, Haffner, & Reynolds (1999) and is an extract of a forthcoming paper which synthesizes multiwavelength data in an attempt to provide a more complete physical description.

The Eridanus superbubble is a huge structure that was produced by the winds and SN of previous generations of Orion stars. The central volume of the

superbubble is full of very hot gas whose spatial structure is well delineated by 0.75 keV X-ray emission, which has a sharp, well-defined edge; we represent the edge with a dashed line on figures that show other gas components. The distance $\sim$ 500 pc and the overall size $\sim 30^\circ$ or 250 pc. The 0.75 keV spatial structure is duplicated by higher-energy very dim 1.5 keV emission. The presence of even a little of this higher energy emission implies a temperature of several million degrees or more, hotter than currently-accepted estimates.

In contrast, the lower-energy 0.25 keV emission (Figure 2, *left*) is brightest near the higher-$|b|$ portions of the superbubble, and also outside its boundary. This outside emission is traditionally thought to come from gas in the Galactic halo. However, we believe that this gas has leaked out of the rear wall of the superbubble and, using 21-cm and Hα-line data, have even been able to locate the specific place where this has happened.

Figure 1 maps the diffuse 100 μm IRAS emission, which traces mainly atomic and molecular hydrogen, and the Hα from the WHAM survey (Haffner, this meeting). All gas phases are prominent in the Eridanus Superbubble: the HIM, which emits the XM emission; the atomic and molecular gas, which sits in the superbubble wall; and the RWIM, which also sits in the superbubble wall.

The Onionskin structure. The lower edge of the superbubble wall, near $b \sim -50^\circ$, has a well-delineated onionskin-type structure, which can be seen by comparing the two panels in Figure 1: the inside layer of the wall is ionized and the outside layer is neutral. This structure is consistent with photoionization caused by the hot Orion stars, because there is little or no neutral gas inside of the bubble and photons stream, unimpeded, from the stars to this high-$|b|$ gas.

Near the middle of the superbubble the photoionization structure takes on a different character. Instead of an onionskin-type structure the walls are either mostly completely ionized or completely neutral. Specifically, over much of the more distant wall of the superbubble the gas is mainly atomic, while the near wall is mainly ionized. This is consistent with the geometry of the OMC region where the dense molecular clouds lie behind the hot stars, so the molecular clouds shield the far wall of the superbubble from the ionizing stellar photons.

In Eridanus, the relationship between the neutral gas and the RWIM is clear. The WIM exists where ionizing photons are able to reach the neutral wall. Indeed, it is difficult to imagine any other source of ionization or energy for the RWIM, so it is natural to extend this concept to all of the WIM: namely, that the RWIM exists in regions that would be occupied by neutral gas were it not for the accidental presence of ionizing photons. These photons ionize and heat the gas, raising its pressure by at least a factor of two.

The electron density and pressure. Heiles et al (1999) derive electron volume densities by comparing the Hα, 21-cm line, and 100 μm intensities. They find typically $n_e \sim 0.8$ cm^{-3}, which corresponds to $\frac{P}{k} = 2n_eT \sim 12000$ cm^{-3} K. This is higher than the pressure of typical CNM clouds, which makes sense because the wall is adjacent to an overpressured HIM region.

We know of one other density determination, namely in the large filament mapped by Haffner, Reynolds, & Tufte (1998). They obtain $n_e \sim 0.18$ cm^{-3}, which corresponds to $\frac{P}{k} \sim 2500$ cm^{-3} K.

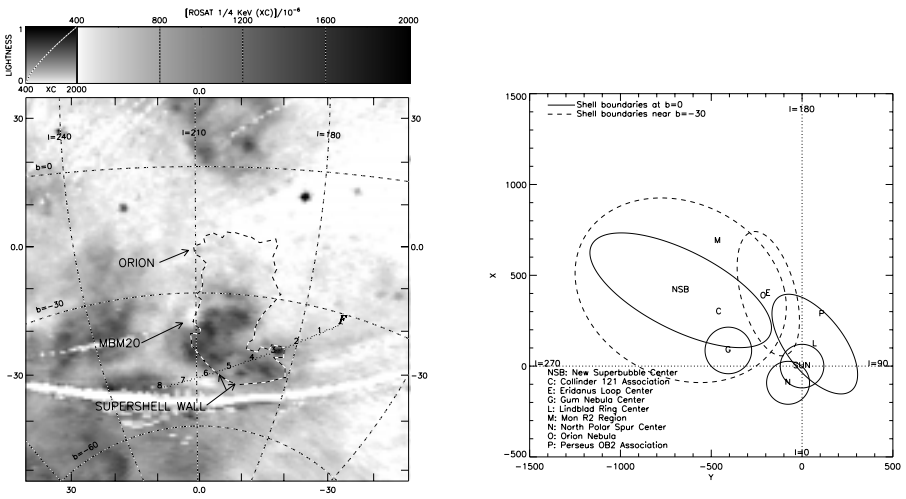

Figure 2. *Left:* The Eridanus region in 0.25 keV X-rays; for details, see the caption for Figure 1. *Right:* Nearby HI shells and bubbles projected onto the Galactic plane, viewed from the north Galactic pole (Heiles 1998). Solid circles or ellipses represent shells near $b = 0°$; dashed ones represent shells near $b \sim -30°$.

3.2. Other prominent nearby superbubbles

We are fortunate in having the textbook example of Eridanus so close and easy to study. However, the probability of this fortunate occurrence is not all that small: the Solar neighborhood is riddled with superbubbles. Another prominent one is the North Polar Spur superbubble (e.g. Egger 1998), which was produced by stars in the Scorpius/Ophiuchus cluster and lies opposite the Eridanus superbubble in the sky. Another is the much older Local Bubble, in which the Sun is immersed. Another is the "New Superbubble" (Heiles 1998), a gigantic old structure centered near $\ell \sim 230°$, which may have been responsible for inducing star formation in the Orion and the Gum regions. And there are numerous others that are older and consequently not very prominent, but whose effects are rather clearly documented in the dynamics of the local gas and in the location of related stellar associations (Bally, this meeting).

RWIM filaments lie on the surface of the Eridanus superbubble. We believe that this also happens for the huge, prominent Haffner et al (1998) RWIM filament, but don't have the space to present this argument. Given these specific examples, we extrapolate and conclude that all prominent RWIM filaments lie on the surfaces of superbubbles in regions where ionizing photons happen to penetrate. Reynolds (1984) also sees a less structured Hα emission component, which corresponds to a more pervasively distributed WIM; this is probably the agglomeration of older versions of the prominent filaments, HII region envelopes, and the MOWIM (partially ionized WNM; §4.1 and 5).

3.3. A superbubble-dominated ISM?

Heiles (1998) provides a map of the local superbubbles, which we reproduce in Figure 2 *right*. They are so numerous that they run into one another and occupy common volumes. This suggests that their HIM's are interconnected, which would mean that the local ISM is superbubble dominated.

However, previous studies find that superbubbles do not occupy a large fractional ISM volume. Observationally, Heiles (1980) uses mainly northern-hemisphere HI data to conclude that the superbubble volume filling fraction is $10 \rightarrow 20\%$. Theoretically, McKee (1993) uses the luminosity distribution of star clusters to calculate the effects of clustered SN and find that the superbubble filling fraction should be $\sim 10\%$.

We can reconcile these seemingly inconsistent conclusions, but not in a way that leads to a definitely preferred choice. If one wants to minimize superbubble dominance, then one argues that some of the objects on Figure 2 are detectable only by fairly weak kinematic signatures, and that they are so old that their interiors no longer contain HIM; also that some are identified only by overinterpretation of the data, and not real.

In contrast, if one wishes to maximize superbubble dominance, then one argues as follows: Observationally, that Heiles (1980) underestimated the filling fraction because he included only northern HI data, missing the most important Galactic quadrant 3, which is in the southern sky and has more obvious superbubble dominance. Theoretically, that McKee (1993) neglects superbubble-shock-induced star formation in which a superbubble shock triggers the formation of additional star clusters. Heiles (1998) believes that Orion/Eridanus and Vela are a result of this process, and this process might occur in the Magellanic Clouds (Oey & Smedley 1998; Points et al 1999). Such correlated cluster formation would produce ISM regions where correlated superbubbles dominate—compensated for by other regions where they don't (because the total rates are, presumably, known).

3.4. The amalgam of densely-packed superbubbles

A young superbubble is a clear, distinct entity. It is rejuvenated by successive SN, and these SN may be produced through successive stellar generations. The superbubble expands and, when the sources of energy finally die out, slows down and merges with the surroundings. The walls remain atomic unless there are sources of ionizing photons; portions of the walls that had been ionized begin to cool and recombine when the sources disappear. The interior HIM cools adiabatically as it expands. An expanding superbubble eventually runs into volume occupied by its neighbors. The walls fragment and become the neutral interstellar clouds. Often a different SN or superbubble shock overtakes such clouds, which then end up inside the remnant bubble as in the MO model and evaporate into the interior HIM (McKee & Cowie 1977).

The interstellar volume becomes an amalgam of all the gas components. The HIM regions should connect and form tunnels as envisioned by Cox & Smith (1974). The neutral gas should form walls of these tunnels and perhaps be embedded within as clouds or fragments. WNM that happens to be immediately adjacent to the HIM is partially ionized by its X-rays, forming the MOWIM. Some of the HI haphazardly turns to RWIM when it is exposed to UV

photons; after the ionizing photons turn off, the RWIM cools and recombines in a time-dependent, nonequilibrium fashion. The walls contain the occasional region where dense molecular gas happens to have formed as a result of shocks, collisions, and random turbulent intermittency (§7).

4. The Two WIM's: RWIM and MOWIM

The WIM is revealed by observations of the diffusely-distributed Hα line (which provides the emission measure $EM = n_e^2 L$) and the dispersion of pulsars (which provides the dispersion measure $DM = n_e L$). There is an additional observational probe: interstellar scintillation/scattering of small diameter radio sources (pulsars and extragalactic nuclei), which is parameterized by the scattering measure SM. The SM is not a simple quantity because it is a measure of interstellar turbulence and small-scale variations in n_e.

The classical assumption is that the WIM consists of a single type of gas—equivalently, that the *same* electrons produce the DM and EM. With this assumption, Haffner et al (1999) use line intensity ratios $\frac{\rm NII}{\rm H\alpha}$ and $\frac{\rm SII}{\rm H\alpha}$ to derive a typical WIM temperature $T \sim 8000$ K. Reynolds et al (1998) use the intensity ratio $\frac{\rm OI}{\rm H\alpha}$ to derive the fractional ionization, typically ~ 0.9 for $T = 8000$ K. These approximate the conditions expected for ionization by the same stellar photons that produce HII regions. This, together with the filamentary morphology, leads us to the picture that much of the WIM resides in filaments lying on superbubble walls, as in Eridanus (§3.1).

However, the data can be also be interpreted using a different assumption, namely that *different* electrons produce the DM and EM. These are the RWIM and the MOWIM. The RWIM is the HII-type WIM discussed just above, and it produces most of the EM (that is, most of the quantity $n_e^2 L$ along any line of sight). The RWIM produces some or most of the Hα and nearly all the collisionally-excited heavy element emission lines. The MOWIM is partially ionized WNM, and produces most of the DM. If the temperature of the MOWIM is low enough, then it can produce significant Hα even with its smaller EM, because the Hα emissivity $\propto T^{-0.9}$.

4.1. The need for two WIM components

In this section we address the need for two WIM components on a global scale. We do this by *assuming, temporarily,* that there is a single WIM component and calculating its typical pressure. This pressure is small compared to that of the CNM, and we argue that this is unlikely. We then go on in the next two sections to discuss the two WIM components.

The single-component WIM pressure WITHOUT Interstellar Scattering Data. Reynolds (1991), in a classic paper, compared DM's of distant high-latitude pulsars with EM's. By assuming that the WIM lies in clouds of average electron density n_a with fluctuations σ, he derived

$$n_a = \frac{EM/DM}{1 + \sigma^2/n_a^2} \tag{1}$$

and used Hα-derived EM's and DM's towards distant pulsars in globular clusters, together with the assumption $\sigma^2 = 0$, to derive $n_a \approx 0.08$ cm^{-3} at $z = 0$. The WIM temperature is about 7000 K, a reliable value if it is in thermal equilibrium and an upper limit if not, so the pressure is $\frac{P}{k} = 2n_eT \lesssim 1100$ cm^{-3} K. This is the typical pressure of the WIM, and it is nearly four times smaller than that of the CNM.

The single-component WIM pressure WITH Intersstellar Scattering Data. Measurements of the Scattering Measure SM show that the WIM's typical pressure is even smaller. There are two types of scattering, diffractive and refractive. The former produces randomly-distributed islands of intense emission in the frequency-time plane, much like terrestrial atmospheric seeing, and the latter produces effects like two-slit interference fringes—correlated islands, much like elongated mountain chains such as the Tetons. Examples of these data are in Stinebring, Faison, & McKinnon (1996) and Gupta, Rickett, & Lyne (1994). These data allow the determination of the turbulence spectrum in the WIM, which is typically very close to being Kolmogoroff. This is a power law with cutoffs at both small and large scales; the large scale cutoff is called the outer scale. TC provide a summary.

Cordes et al (1991) interpret these data in a classic paper. The fluctuations that produce the observed scattering are tiny in size, $\sim 10^5$ km, but there are good reasons to extrapolate the inferred turbulence spectrum to larger size scales. Moreover, the refraction scattering is pronounced and is produced by larger (but still tiny: a few AU) fluctuations; this indicates that the spectrum is even steeper than Kolmogoroff. The result is that the outer scale of the turbulence spectrum is inferred to extend all the way up to the size of the clouds and this means that, in equation 1, one should take $\frac{\sigma_a^2}{n_a^2} \sim 1$. This decreases n_a still further, by a factor 2 to about 0.04 cm^{-3}, so the typical pressure in the WIM clumps becomes only $\frac{P}{k} \lesssim 600$ cm^{-3} K.

Commentary: WIM pressure and the two WIM's. One might not be surprised at a systematic difference in thermal pressure between the WIM and the CNM. However, I think one should be surprised if the typical WIM pressure were systematically *smaller* than the typical CNM pressure, particularly by such a large factor. We think of the single-component WIM as portions of neutral shell walls, or fragments thereof, that happen to have been exposed to ionizing stellar photons—and when the neutral medium is ionized, its pressure increases by at least a factor of two. This idea is strengthened by the observations of the filaments quoted in §3.1.

Let us suppose for the moment that the WIM pressure follows our intuitive expectation and is significantly larger than the 600 cm^{-3} K. We derived the pressure using equation 1; increasing the pressure requires changing the ratio $\frac{EM}{DM}$. The only way to accomplish this is to assume that most of the observed DM comes from a different electron component than the EM. To retain approximate thermal pressure equality, this component must contribute most of the observed DM and less of the observed EM, which pulls it towards lower n_e; yet, in conflict, we want it to have a higher pressure. The only way out is to embed the electrons in one of the primarily neutral phases. The only reasonable such phase is the WNM, because only it has small enough n_{HI} to allow the needed n_e.

Commentary: the RWIM and the MOWIM. Thus, we identify the MOWIM with a partially ionized portion of the WNM. This means that portions of the WNM must have significant fractional ionization with $X_e \gtrsim 0.1$. Our identification is not the first observational indication of this association. Indeed, Spitzer & Fitzpatrick (1993; SF93) have already made this suggestion on the basis of UV absorption line data towards HD93521. Moreover, the local cloud adjacent to the Solar system has $X_e \sim 0.5$ (Redfield & Linsky 2000; RL). However, these measurements are for individual regions; what's new here is our claim that the MOWIM is *globally* important.

Our argument suggests that the MOWIM provides most of the pulsar DM's. It also suggests one observationally important item (Spangler 1991), which was brought to my attention by Cordes and Zweibel (private communication). The degree to which the interstellar electrons produce scattering fluctuates widely with position (Cordes et al 1991, TC). The turbulence that produces the scintillation exists at such small scales exists because of transfer of turbulent energy from large to small length scales (Goldreich & Sridhar 1995). The turbulence is damped by ion-neutral collisions, whose importance increases to a saturated value at small length scales. It is possible that the larger neutral content in the MOWIM reduces the small-scale turbulence enough to render it ineffective for interstellar scattering, leaving the RWIM as the primary scattering medium.

5. The MOWIM: Partially Ionized WNM

In this section we discuss observations of the WNM and its fractional ionization in specific regions. Some of these support the idea of the MOWIM.

5.1. The Dispersion Measure Imperative Assumption (DIMP)

In §4.1 we introduced the MOWIM and suggested that portions of the WNM are nontrivially ionized, contributing significantly to the pulsar DMs. Unfortunately, this idea is hard to test because the optical/UV line data do not provide direct measurements of ionization fraction for situations where n_{HI} is small, as in the WNM. What they *do* provide is direct measurements of n_e; the trick is to somehow obtain n_{HI} values to associate with these n_e measurements. We will accomplish this with the Dispersion Measure Imperative Assumption.

Fitzpatrick & Spitzer (1997, FS) is the culmination of an excellent series of four optical/UV absorption line studies of high-latitude gas. The optical/UV data provide electron volume densities n_e at a sensitive level: for WNM components having $N_{HI,20} \gtrsim 0.1$, FS detect n_e as small as 0.02 cm^{-3}. They also detect one ionized component with $N_{e,20} \sim 1.3$ and $n_e \sim 0.2$ cm^{-3}. These numbers suggest that FS can reliably detect *all* the interstellar electrons over the ranges of volume and column density that are relevant for DM and EM studies.

We believe the DM-producing electrons to be pervasive. Thus, they should exist on every sightline. Because of the sensitivity of the FS data to electrons, FS should detect the DM-producing electrons on *every sightline*. They don't find fully-ionized components, except for one probably isolated small HII region. Thus one is drawn toward the *DM-Imperative Assumption*, or *DIMP*:

We assume the WNM components to contain all the electrons required for pulsar DM. This means that we assume each component to have the global ratio

of column density $\frac{n_e}{n_{WNM}} = \frac{N_{e\perp}}{N_{WNM\perp}} \sim \frac{0.5}{1.9}$ (from Table 1); this corresponds to $X_e = 0.21$. N_{HI} and n_e are both known for some components, so we obtain n_{HI}—and then the total thermal pressure.

Of course, this assumption is extreme. First, MO predict the ionization fraction of the WNM to be highly variable: it depends on the exposure to soft X-rays, which are atteunuated by small HI column densities. Second, it doesn't include the DM contribution of the conventional, fully-ionized RWIM.

5.2. Discussion of specific stars

The HD93521 sightline. The HD93521 sightline (SF93) contains no CNM (except one insignificantly small component with $N_{HI,20} = 0.06$): the coldest gas component has upper limit $T \lesssim 540$ K, and most of the other temperature upper limits are in the range $T \lesssim 4800 \rightarrow 6900$ K with derived $n_e = 0.055 \rightarrow 0.11$ cm^{-3}. From the DIMP assumption we obtain typically $n_{HI} \sim 0.2 \rightarrow 0.43$ cm^{-3}, yielding total thermal pressures $\frac{P}{k} \sim 2000 \rightarrow 4000$ cm^{-3} K.

Our quick discussion underscores the important conclusion of SF93: along this sightline at least, *the DM-producing electrons reside in the WNM.* The only way to negate this conclusion is to reduce X_e from its assumed value of 0.21. However, this raises n_{HI} and causes the thermal pressures to be much higher than a few thousand cm^{-3} K, which would make them exceed the upper limit for WNM in the Wolfire et al (1995a; WHMTB) model. Slavin, McKee, & Hollenbach (2000) account very well for the HD93521 observations with soft X-ray photons from old SN remnants.

The HD215733 sightline. This sightline (FS) has only one useful WNM component, which has $T = 730 \pm 70$ K (a value, not an upper limit) and $n_e = 0.07$ cm^{-3}. The DIMP assumption gives $n_{HI} = 0.27$ cm^{-3} and thermal pressure $\frac{P}{k} = 300$ cm^{-3} K. The density is about ten times smaller than the pressure-equilibrium value at $T = 730$ K.

If instead the thermal pressure is $\frac{P}{k} = 3000$ cm^{-3} K, then $n_{HI} \sim 4.1$ cm^{-3}, about twice the equilibrium value for $T = 730$ K. The ionization fraction is $X_e \sim 0.017$, about 5 times higher than equilibrium in the standard model of WHMTB.

In terms of the MO paradigm of pressure equilibrium, the latter possibility is much more reasonable. But then we must ask, "Where do the pulsar-DM electrons reside?" Perhaps this sightline has a very small DM?

The HD149881 sightline. In contrast to the others, this sightline (Spitzer & Fitzpatrick 1995; SF95) contains a truly ionized component. However, SF95 interpret it as a small HII region, probably produced by HD149881 itself. Such HII regions are presumably rare, so the assumption that the DM-producing electrons are pervasive still applies to the neutral components along this sightline.

This star has three WNM components with $T \sim (6000, 840, 2000)$ K. We quote their Na-determined electron densities, which we regard as more reliable than the Ca values because the depletion of Na is less variable. The quoted electron densities are lower limits because of the assumption that Na is undepleted. SF95 provide values for only the first and third components; they are $n_e \gtrsim (0.049, 0.018)$ cm^{-3}.

The DIMP assumption gives $n_{HI} = (0.19, 0.069)$ and $\frac{P}{k} = (1700, 200)$ cm^{-3} K. The first component is in reasonable agreement with thermal equilibrium. The second component suffers incompatibility with equilibrium to a similar extent as the HD325733 component.

The Colorado Model of the Local Interstellar Cloud. The local cloud just adjacent to the Solar system has well-determined properties: $n_{HI} = 0.10$ cm^{-3}, fractional ionization $X_e = 0.52$ (exceeding the DIMP assumption!), and $T \sim 7000$ K. These combine to give the relatively high value $\frac{P}{k} \sim 2200$ cm^{-3} (RL).

5.3. Commentary on WNM ionization

The DIMP assumption works well for the first star, HD93521, and also for the Local Interstellar Cloud. It also works reasonably well for the first component of HD149881. We conclude that along some sightlines, and in some WNM clouds, the DM-producing electrons reside primarily in the WNM instead of the standard WIM. In other words, we concude that the MOWIM really does exist and might be globally important.

In ionization equilibrium the total H-ionization rate is $\zeta_{-15} = n_{HI} \left(\frac{X_e}{0.05}\right)^2$ (KH, section 6.4), where ζ_{-15} is the total H-ionization rate in units of 10^{-15} s^{-1}. Taking $X_e = 0.2$ and $n_{HI} = 0.3$, these WNM components have $\zeta_{-15} \sim 5$. This seems very high, but the MO model has it much higher, $\zeta_{-15} \sim 110$; it comes from soft XR emitted by the adjacent HIM, and is attenuated very rapidly going inside the cloud because of absorption by the HI.

This conclusion, that significant DM-producing electrons reside in the WNM, is precisely opposite to that of section 6.4 of KH. Their conclusion was based on the assumptions of thermal pressure equality, equilibrium for both temperature and ionization, and much smaller values of ζ_{-15} based on observations of dense clouds. The optical/UV absorption line data make it clear that those assumptions are not universally valid!

The DIMP assumption works much less well for HD215733 and the second component of HD149881 because it produces small values for HI volume density and thermal pressure; we instinctively rebel against such small values because they are so far from conventional ones. Both these components have $T \sim 800$ K. This is an awkward temperature for equilibrium models because it is in the thermally unstable region. If one prefers to discard the DIMP assumption for these components, then the physical parameters are closer to conventional values. However, then one must ask where the DM-producing electrons reside on these sightlines. Perhaps the answer is that these sightlines don't contain the expected electron column densities, with the possible ramification that the DM-producing electrons are not very pervasive.

If, instead, these awkward components do contain a significant fraction of the DM-producing electrons, then they (and presumably many others) are greatly thermally underpressured with respect to their surroundings. This doesn't necessarily mean that the *total* pressures in these structures are small, because generally speaking macroscopic motions, magnetic field, and cosmic rays contribute most of the interstellar pressure. Perhaps the implied strong field strengths explain the relatively large values of rms magnetic field strength determined from studies of DM fluctuations (see reviews by Heiles 1995, 1996).

6. New Observations of the CNM and WNM

6.1. Temperatures from New 21-cm Line Observations

Tom Troland and I have been pursuing an intensive observational program to measure properties of the CNM and WNM using 21-cm line emission/absorption line observations at Arecibo Observatory, the details of which will be forthcoming in future papers[1]. Our interpretation is new because we assume clouds of uniform temperature and we perform a physically self-consistent treatment of the radiative transfer, with excellent results.

The absorption spectra consist of very obvious velocity components and we represent their optical depths by Gaussians. We decompose the associated emission profile into two sets of Gaussians: (1) a set with the same centers and widths as the absorption profile's Gaussians; and (2) one or two additional Gaussians to make up the difference. The former set is the CNM and the latter the WNM. Interesting details include considering the fraction of WNM that lies in front of the CNM and, also, the relative ordering along the line of sight of the CNM components—nearby ones absorb the more distant ones. For most sources the CNM components plus one or two WNM components produce a very good fit.

We show the results for 3C18, which is one of the simplest profiles and good for an illustrative example. Figure 3A is the absorption spectrum. The solid line is the observed absorption spectrum, which we fit with the three CNM components whose depths and halfwidths are indicated; the dash-dot line is the fit, which is almost indistinguishable from the data. Figure 3B is the emission spectrum. The solid line is the observed profile, which we fit with *(1)* the amplitudes of the three absorption Gaussians, keeping their centers and widths fixed; plus *(2)* a single WNM component. The dashed curve is the contribution to the emission spectrum from the absorption components and the dotted curve the contribution from the WNM component, which is unabsorbed by the CNM because we take all the WNM as lying in front the CNM, which placement provides the lowest residuals. The full fitted curve is the sum, shown as dash-dot, which is a good fit.

The WNM component has halfwidth 10.0 km s^{-1}, which corresponds to purely thermal broadening at $T = 2200$ K; this is an upper limit on the kinetic temperature. For the three CNM components, left-to-right on Figure 3A, the spin temperatures are 46 ± 9, 43 ± 6, and 32 ± 1 K; their Zeeman splittings (data not shown) give line-of-sight field strengths 0.3 ± 12.1, 10.7 ± 5.8, and -3.6 ± 1.6 μG.

The WNM component contributes $N_{HI,20} = 3.2$ and the three CNM components $N_{HI,20} = 1.8$, where $N_{H,20}$ is the HI column density in units of 10^{20} cm^{-2}. The WNM/CNM ratio is ~ 1.8, significantly higher than the average of ~ 1. About half the HI is WNM, much higher than the MO predicted fraction of ~ 0.04.

[1] I emphasize that the results presented here are provisional and will change in detail (but hopefully only in detail!).

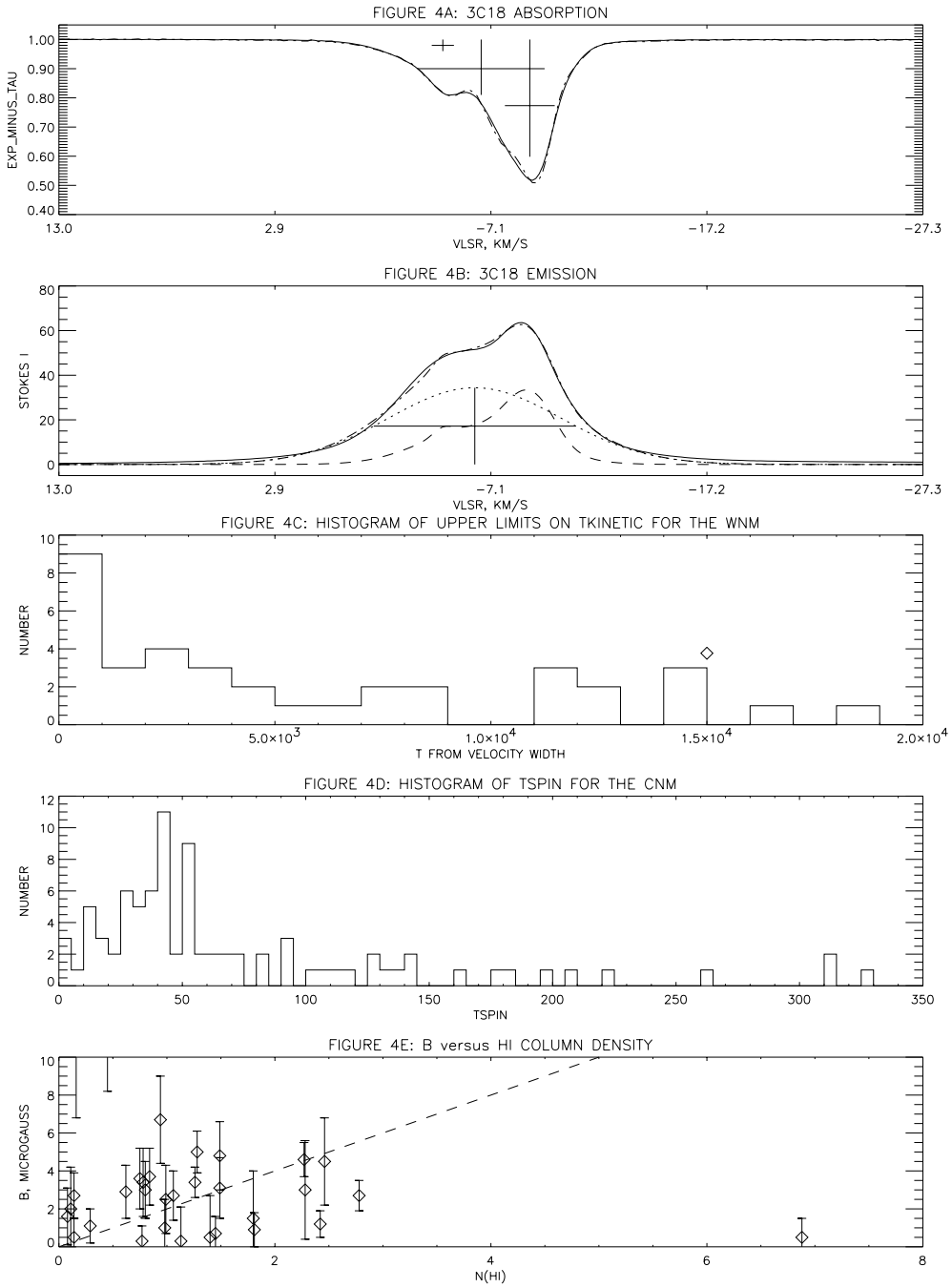

Figure 3. **A** and **B** exhibit the 21-cm line absorption and emission towards 3C18; the solid line is data and the dash-dot line the fit. Crosses indicate Gaussian component parameters. In **B** the dashed line illustrates the contribution from the three CNM components and the dotted line the WNM component. **C** is the histogram of upper limits on kinetic temperature for the WNM components and **D** the histogram of spin temperatures of the CNM components. **E** plots the observed line-of-sight magnetic field strength versus HI column density (units: 10^{20} cm^{-2}) for the CNM components.

6.2. Temperatures from optical/UV absorption line observations

For kinematic studies, optical/UV absorption line studies of high-latitude gas have the advantage that the thermal broadening of heavy elements is small, so closely-spaced velocity components are more distinctly revealed than with the 21-cm line. Their disadvantage is that derived temperatures aren't very accurate because they are obtained by comparing heavy-element and HI linewidths; the HI line comes from a much larger angular area so the nonthermal component of its width may be larger than that of the heavy element lines, raising the derived temperatures above the actual ones. In particular, optical/UV temperatures for CNM gas are not at all accurate.

One principal result of FS is that each Gaussian that one would fit to a 21-cm emission line consists, in the optical/UV absorption line data (and thus reality), of a superposition of several closely-spaced components. The relation between the optical/UV lines and the 21-cm emission line is much like that between the 21-cm absorption and emission lines for 3C18 in Figure 3A: the separations and widths are not dissimilar. It is natural, then, to assume that the 21-cm absorption line data represent the complete picture of CNM gas. It would be nice to confirm this by using exactly the same sightlines for the radio and optical measurements.

6.3. TEMPERATURE OF THE WNM

The new 21-cm line data. The WNM Gaussian widths provide upper limits for kinetic temperature T_K. Figure 3C exhibits a histogram of these limits. About half the components have $T_K < 5000$ K; because these components are not visible in absorption, their spin temperatures exceed ~ 500 K. This range, $500 \rightarrow 5000$ K, is the thermally unstable range that separates CNM from WNM.

Our Arecibo data show this departure from thermal stability in a statistically convincing manner. Previous studies have hinted at this result. In emission/absorption studies, Mebold et al (1982) decomposed emission line profiles into Gaussians, with similar results; however, they didn't explicitly point out this departure. Verschuur & Magnani (1994) and Heiles (1989) analyzed emission profiles and found pervasive components with widths in this range, but without absorption data could not conclusively state that the kinetic temperatures were indeed so high.

The FS and Colorado data. FS derive WNM temperatures by comparing heavy-element and HI linewidths; we restrict our summary to those WNM components having $N_{HI,20} > 0.1$ that also have well-determined temperatures or upper limits. The character of their results depends on the particular sightline.

For HD93521 $[(\ell, b) = 183°, 62°)]$ they found four components, all with high upper limits on kinetic temperature $\lesssim 4900 \rightarrow 6900$ K. For HD149881 $[(\ell, b) = 31°, 36°)]$ they found two components with kinetic temperatures 840 ± 150 and 2000 ± 400 K. For HD215733 $[(\ell, b) = 85°, -36°)]$ they found two components with kinetic temperatures 730 ± 70 and 2500 ± 280 K. Finally, the Local Interstellar Cloud has $T \sim 7000$ K and $\frac{P}{k} \sim 2200$ cm^{-3} (RL).

Commentary on WNM temperature We conclude that many WNM components are in the thermally unstable temperature range. Pressures in the WNM appar-

ently have wide variations: the Local Cloud and the sightline towards HD93520 are characterized by $\frac{P}{k}$ in the thousands, while the other two have much lower temperatures and might have $\frac{P}{k}$ in the hundreds if the DIMP assumption of §5.1 applies. Thermally unstable temperatures should not often occur in the MO model, and such low pressures should be rare.

The isobaric stability criteria don't necessarily apply in an obvious way to the WNM. WNM structures have low densities, $n_{HI} \sim 0.1 \rightarrow 0.4$ cm^{-3} for the FS's five WNM components towards HD93521 (§5.2), and should occupy relatively long lengths along the sightline, tens of pc, so the sound crossing time should be comfortably longer than the thermal cooling time.

WHMTB find Lyα cooling to dominate the WNM, even at the low fractional ionizations that occur in equilibrium. If the ionization fractions are as large as required for the DIMP assumption in §5.1 to be valid, meaning that the DM-producing electrons do indeed occur in the WNM, then some Hα lines in the WHAM survey should have parallels in the 21-cm line emission from low-temperature WNM/MOWIM.

6.4. Temperature of the CNM

For the CNM, spin temperature is the same as kinetic temperature. Figure 3D exhibits the histogram of derived spin temperatures for all CNM components. Most components have $T_S < 75$ K. This is in marked contrast to previous results, where histograms had broad peaks over the ranges $20 \rightarrow 140$ K (Mebold et al 1982) and $50 \rightarrow 300$ K (Dickey, Salpeter, & Terzian 1978, DST; Payne, Salpeter, & Terzian 1982, PST). Our range is narrower and there is a suggestion that the histogram is doubly peaked, with one peak in the range $10 \rightarrow 20$ K and the other $30 \rightarrow 75$ K.

Consider first the higher temperature $30 \rightarrow 75$ K range. This agrees very well with theory. WHMTB included all known processes in calculating their standard model, for which the CNM equilibrium temperatures range from $25 \rightarrow 200$ K (the corresponding densities are $n_{HI} \gtrsim 1000 \rightarrow 4$ cm^{-3}). Our observed temperature range is smaller and corresponds to $n_{HI} \gtrsim 250 \rightarrow 20$ cm^{-3} and $\frac{P}{k} = 10000 \rightarrow 1500$ cm^{-3} K. These numbers are in accord with current ideas about the CNM.

Modern theoretical models do not predict our low-temperature $10 \rightarrow 20$ K range. However, the theoretical interpretation of such low temperatures is actually quite straightforward. In the days when Spitzer (1978) wrote his famous textbook, heating by photoelectric emission from dust grains was not a well-accepted process and Spitzer calculated the CNM equilibrium temperature assuming that only the classical mechanisms prevailed, namely heating by photoionization of Carbon and cooling by electron recombination onto ionized Carbon. The equilibrium temperature is 16 K and is independent of the abundance of Carbon and of the starlight intensity. This is precisely in the middle of our low-temperature range!

In order that CNM gas *not* be heated by photoelectric emission from grains, the gas cannot contain grains—more specifically, the gas cannot contain the particular kinds of grain that heat the gas. In WHMTB's theory, these are small grains ($\lesssim 300$ Å) and PAH's. It seems difficult to produce gas without such grains. One cannot rely on strong shocks, because they add to the small-

grain population by shattering large grains (Jones, Tielens, & Hollenbach 1996). It seems that one must destroy all the grains, perhaps by cycling the gas through the HIM phase, or let the CNM cloud sit quiescentally for a long time so that small grains coagulate into large ones.

These parcels of very cold gas shouldn't contain small grains and PAH's! This prediction can be checked observationally from far-IR emission maps, and perhaps from Ca absorption lines (gaseous Ca is usually rare in the ISM because of depletion onto dust grains). Such cold gas was invoked by Heiles (1997) to help understand the existence of tiny-scale atomic structure; the observed existence of such cold gas is encouraging for that interpretation.

The Morphology of the CNM. Typical Gaussian components of the CNM contain $N_{HI,20} \sim 1$. Consider a CNM cloud having $n_H = 100$ cm^{-3}. If it is spherical, then its diameter is 0.3 pc. The scale height of the CNM is ~ 100 pc, so our CNM cloud is typically at $\frac{50}{\sin(b)}$ pc distance and occupies angle $\sim \frac{20}{\sin(b)}$ arcmin. This is uncomfortably close to the Arecibo beam diameter. Nevertheless, DST and PST found that most of the emission fluctuations occur on larger angular scales, and our Gaussian decompositions show that roughly half of the total emission comes from the CNM. Moreover, FS find good correspondence between optical/UV components along the sightline to a star and 21-cm line emission components observed with a 20 arcmin beamwidth. This is somewhat of a conflict.

It makes sense to drop the idea of spherical clouds; there is much evidence for nonspherical structures in the ISM. To resolve the conflict, CNM structures need to be relatively large across the line of sight compared to along the line of sight. This can be achieved if their morphologies are sheetlike. This makes sense from another aspect: the CNM is supposed to be formed by shocks.

Magnetic field strengths in the CNM. Even for "neutral" atomic gas there is plenty of residual ionization to satisfy flux freezing over many tens of Myr. Accordingly, the magnetic field strength should be large in the CNM: both the gas and also the magnetic field have been swept up from within the entire volume of the superbubble. This idea is confirmed by observed large field strengths, ~ 10 μG, which are observed in gas that resides in morphologically obvious superbubble walls (Heiles 1989; Myers et al 1995).

Our current Zeeman splitting measurements apply not to obvious supershell walls, but rather to sightlines towards radio sources and are thus randomly selected. We measure very low field strengths or upper limits, typically no more than a few μG. Figure 3E plots observed field strength versus $N_{HI,20}$ for these CNM Gaussian components, together with a dashed line that represents the approximate boundary between magnetism dominating gravity for self-gravitating clouds (which may be completely irrelevant: gravity plays no role in these clouds). All points having $N_{HI,20} > 1.5$ fall below the line. Moreover, most of the reliably measured points have $B \lesssim 4$ μG, in marked contrast to the ~ 10 μG field strengths in morphologically obvious supershell walls. "Morphologically obvious" means that the walls are seen edge-on; in contrast, the random lines of sight preferentially sample sheets (§6.4) that are *not* edge on.

The new CNM field strengths are not higher than the volume-average field strength of about 5 μG derived from various observations independently by Heiles (1996) and Ferrière (1998). The volume densities that characterize this

volume-averaged field are very small, much smaller than the $n_{HI} \gtrsim 100$ cm^{-3} of our CNM clouds. With flux freezing, field strength should increase with volume density. Thus flux freezing doesn't apply to these randomly-chosen CNM clouds. Our result, that the CNM does not necessarily contain high magnetic fields, is consistent with the analysis of other observations by Padoan & Nordlund (1999).

7. The Turbulent ISM

MO dealt with turbulence by considering how interstellar clouds as discrete entities would be buffeted by passing SN shocks, much as ocean waves toss jellyfish about. A number of recent numerical experiments emphasize a different type of turbulence which has no discrete entities, but instead has continuous distributions of physical parameters, much as waves beating on a rocky headland produce relative fluid motions with localized, temporary regions of high vorticity or velocity dispersion; cloud boundaries are arbitrary surfaces that dissipate with time (e.g. Ballesteros-Paredes, Vázquez-Semadeni, & Scalo 1999; Smith, Mac Low, & Heitsch 2000; Padoan & Nordlund 1999; Vázquez-Semadeni, Gazol, & Scalo 2000). The state of the CNM and WNM is not completely controlled by the standard phase diagram, but also by the vissicitudes of turbulent flow. The numerical experiments include most relevant physics, including magnetic fields, but are two-dimensional.

I find the numerical experiments attractive. Observations make it clear that turbulence is important in the ISM on a wide range of scales, from tiny (interstellar scattering, §4.1) to huge (supershells). To the eye, the pictorial results of the numerical experiments actually look like the data—an excellent beginning, but insufficient for quantitative comparison. This is quite a contrast from the MO concept of shocks overtaking self-contained clouds whose mass stays inside the boundaries.

Extreme departures from average conditions are known as intermittency. To my knowledge, this was introduced to astronomy in an observational context as broad, nonthermal line wings by Falgarone & Phillips (1990) and in interpretive and theoretical contexts by Falgarone & Puget (1995) and Falgarone, Pineau Des Forets, & Roueff (1995). Intermittency produces highly variable, non-Gaussian distributions in space and time of velocity, vorticity, temperature, and other physical variables. The short-lived extreme conditions can produce observed nonthermal motions, can decouple grains and gas, and can initiate chemical reactions.

These numerical experiments have only recently begun and it is too soon to say that they really do describe the observations better than the MO paradigm. We look forward to further developments in this field because it offers a new vista in comparing with observations, and the comparisons seem to be favorable.

8. The McKee/Ostriker Model: Paradigm?

At the first Tetons meeting, KH reviewed the observations in terms of the MO model with great success. How do things stand now? Here is my personal view, not necessarily shared by others:

- **HIM:** MO works well—a plus (§2.1).

• **RWIM:** Although MO doesn't predict this, others do and this is not necessarily a negative for MO (§2.2, 4).

• **MOWIM:** We suggest that this partially-ionized WNM, which produces pulsar DM but not much else including interstellar scattering, exists globally. This is contrary to most current observational thought. MO predicts this component—a big plus (§2.3, 4.1).

• **WNM mass:** MO predict this to be a minor part of the ISM. Observations show that its mass is equal to, perhaps more than, the CNM—a minus (§6.1).

• **WNM temperatures:** Our new 21-cm line data show that significant portions of WNM are below 5000 K and thermally unstable—a big minus (§6.3).

• **CNM temperatures:** The new CNM temperatures agree well with MO—a plus (§6.4).

• **CNM morphology:** We argue that the CNM is sheetlike, not spherical as envisioned by MO—a minus (§6.4).

• **Magnetic fields and cosmic rays:** MO don't include these in their theory. Their pressures are high and presumably they have a big effect (§1).

• **Turbulence:** It is not clear to me how turbulence relates to MO (§7).

• **Net Score:** One big plus and one big minus. Two plusses and two minuses. Some questions on things not included. Of course, high-quality data are sparse and much of our discussion is based on unpublished data. Does all this make the MO model a paradigm?

Acknowledgments. It is a pleasure to acknowledge conversations with John Dickey, Alex Lazarian, Pablo Padoan, and Enrique Vázquez-Semadeni. Discussions with Jim Cordes, Jeff Linsky, and Ellen Zweibel were especially helpful and stimulating, resulting in a great improvement on the first draft of this paper. The prize goes to Chris McKee, who responded to the first draft with a huge set of comments that not only reversed some of my misconceptions regarding MO but also stimulated new ideas; however, this certainly does not mean that my understanding of MO is complete or that he endorses all opinions expressed herein!

This work was partly supported by NSF grant AST9530590 to the author.

References

Anantharamaiah, K.R. 1985, J. Astr. Ap, 6, 203.

Anantharamaiah, K.R. 1986, J. Astr. Ap, 7, 131.

Ballesteros-Paredes, J., Vazquez-Semadeni, E., & Scalo, J. 1999, ApJ, 515, 286.

Boulares,A. & Cox, D.P. 1990 ApJ, 365, 544.

Cordes, J.M., Weisberg, J.M., Frail, D.A., Spangler, S.R., & Ryan, M. 1991, Nature, 354, 121.

Cox, D.P. & Smith, B.W. 1974, ApJ, 189, L105.

Cox, D.P. 1995, in The Physics of the Interstellar Medium and Intergalactic Medium, ASP Conference Series Volume 80, ed. A. Ferrara, C.F. McKee, C. Heiles, P.R. Shapiro, p. 317.

Dalgarno, A. & McCray, R. 1972, ARAA, 10, 375.

Dickey, J.M., Salpeter, E.E., & Terzian, Y. 1978, ApJS, 36, 199 (DST).

Dixon, W.V.D., Davidsen, A.F., & Ferguson, H.C. 1996, ApJ, 465, 288.

Dove, J.B. & Shull, J.M. 1994, ApJ, 430, 222.

Egger, R. 1998, in The Local Bubble and Beyond, IAU Colloq No. 166, ed D. Breitschwerdt, M.J. Freyberg, J. Trümper, Springer-Verlag (Berlin), p. 287.

Elmegreen, B.G. 1994, in The First Symposium on the Infrared Cirrus and Diffuse Interstellar Clouds, ASP Conf Series 58, ed R.M. Cutri & W.B. Latter, p. 380.

Falgarone, E. & Phillips, T.G. 1990, ApJ, 359, 344.

Falgarone, E., Pineau Des Forets, G., & Roueff, E. 1995, A&A, 300, 879.

Falgarone, E. & Puget, J.L. 1995, A&A, 293, 840.

Ferrière, K. 1998, ApJ, 497, 759.

Field, G.B., Goldsmith, D.W., & Habing, H.J. 1969, ApJ, 155, L149 (FGH).

Fitzpatrick, E.L. & Spitzer, L. 1997, ApJ, 475, 623 (FS).

Goldreich, P. & Sridhar, S. 1995, ApJ, 438, 763.

Gupta, Y., Rickett, B.J., & Lyne, A.G. 1994, MNRAS, 269, 1035.

Haffner, L.M., Reynolds, R.J., & Tufte, S.L. 1998, ApJ, 501, L83.

Haffner, L.M., Reynolds, R.J., & Tufte, S.L. 1999, ApJ, 523, 223.

Hartmann, Dap, & Burton, W.B. 1997, Atlas of Galactic Neutral Hydrogen, Cambridge University Press.

Heiles, C. 1980, ApJ, 235, 833

Heiles, C. 1989, ApJ, 336, 808.

Heiles, C. 1994, ApJ, 436, 720.

Heiles, C. 1995, in The Physics of the Interstellar Medium and Intergalactic Medium, ASP Conference Series Volume 80, ed. A. Ferrara, C.F. McKee, C. Heiles, P.R. Shapiro, p. 507.

Heiles, C. 1996, in Polarimetry of the Interstellar Medium, ASP Conference Series Volume 97, ed. W.G. Roberge & D.C.B. Whittet, p 457.

Heiles, C. 1997, ApJ, 481, 193.

Heiles, C. 1998, ApJ, 498, 689.

Heiles, C., Haffner, L.M., & Reynolds, R.J. 1999 New Perspectives on the Interstellar Medium, Astronomical Society of the Pacific Conference Series 168, p 211.

Jenkins, E.B., Jura, M., & Lowenstein, M. 1983, ApJ, 270, 88.

Jones, A.P., Tielens, A.G.G.M., & Hollenbach, D.J. 1996, ApJ, 469, 740.

Kulkarni, S.R. & Heiles, C. 1987, in Interstellar Processes, ed. D. J. Hollenbach & H.A. Thronson, Reidel, Dordrecht, p 87 (KH).

Martin, C. & Bowyer, S. 1990, ApJ, 350, 242.

Matsuhara, H. et al 1997, ApJ, 490, 744.

McCray, R. & Snow, T.P. 1979, ARAA, 17, 213.

McKee, C.F. 1993, in Back to the Galaxy, AIP Conf Proc 278, ed. S.S. Holt & F. Verter, 499.

McKee, C.F. & Cowie, L.L. 1977, ApJ, 215, 213.

McKee, C.F. & Ostriker, J.P. 1977, ApJ, 218, 148 (MO).

McKee, C.F. & Williams, J.P. 1997, ApJ, 476, 144.

Mebold, U., Winnberg, A., Kalberla, P.M.W., & Goss, W.M. 1982, A&A, 115, 223.

Miller, W.M. & Cox, D.P. 1993, ApJ, 417, 579.

Myers, P.C., Gooman, A.A., Güsten, R., & Heiles, C. 1995, ApJ, 442, 177.

Nakagawa, T. et al 1998, ApJS, 115, 259.

Oey, M.S. & Smedley, S.A. 1998, AJ, 116, 1263.

Padoan, P. & Nordlund, Å1999, ApJ, 526, 279.

Parker, E.N. 1966, ApJ, 145, 811.

Payne, H.E., Salpeter, E.E., & Terzian, Y. 1982, ApJS, 48, 199 (PST).

Points, S.D., Chu, Y.H., Kim, S., Smith, R.C., Snowden, S.L., Brandner, W., & Gruendl, R.A. 1999, ApJ, 518, 298.

Redfield, S. & Linsky, J. 2000, ApJ, 534, 825 (RL).

Reynolds, R.J. 1984, ApJ, 282, 191.

Reynolds, R.J. 1991, ApJ, 372, L17.

Reynolds, R.J., Haffner, L.M., & Tufte, S.L. 1999, ApJ, 525, L21.

Reynolds, R.J., Hausen, N.R., Tufte, S.L., & Haffner, L.M. 1998, ApJ, 494, L99.

Schlegel, D.J., Finkbeiner, D.P., & Davis, M. 1998, ApJ, 500, 525.

Shelton, R.L. & Cox, D.P. 1994, ApJ, 434, 599.

Slavin, J.D., McKee, C.F., & Hollenbach, D.J. 2000, ApJ, in press.

Smith, M.D., Mac Low, M., & Heitsch, F. 2000, A&A, in press.

Snowden, S.L. et al 1997, ApJ, 485, 125.

Spangler, S.R. 1991, ApJ, 376, 540.

Spitzer, L. 1978, Physical Processes in the Interstellar Medium, Wiley: New York, p. 143.

Spitzer, L. & Fitzpatrick, E.L. 1993, ApJ, 409, 299 (SF93).

Spitzer, L. & Fitzpatrick, E.L. 1995, ApJ, 445, 196 (SF95).

Stinebring, D.R., Faison, M.D., & McKinnon, M.M. 1996, ApJ, 460, 460.

Taylor, J.H. & Cordes, J.M. 1993, ApJ, 411, 674 (TC).

Vázquez-Semadeni, E., Gazol, A., & Scalo, J. 2000, ApJ, submitted.

Verschuur, G.L. & Magnani, L. 1994, AJ, 107, 287.

Wolfire, M.G., Hollenbach, D., McKee, C.F., Tielens, A.G.G.M., & Bakes, E.L.O. 1995a, ApJ, 443, 152 (WHMTB).

Wolfire, M.G., McKee, C.F., Hollenbach, D., & Tielens, A.G.G.M. 1995b, ApJ, 453, 673.